EUROPEAN ORGANIZATION FOR NUCLEAR RESEARCH

CERN-PH-EP/2007-004
21 February 2007

# First observation and branching fraction and decay parameter measurements of the weak radiative decay $\Xi^0 \to \Lambda e^+ e^-$

NA48 collaboration

J.R. Batley, G.E. Kalmus [1], C. Lazzeroni, D.J. Munday, M. Patel, M.W. Slater, S.A. Wotton

*Cavendish Laboratory, University of Cambridge, Cambridge, CB3 0HE, U.K.* [2]

R. Arcidiacono [3], G. Bocquet, A. Ceccucci, D. Cundy [4], N. Doble [5], V. Falaleev, L. Gatignon, A. Gonidec, P. Grafström, W. Kubischta, I. Mikulec [6], A. Norton, B. Panzer-Steindel, P. Rubin [7,*], H. Wahl [8]

*CERN, CH-1211 Genève 23, Switzerland*

E. Goudzovski [5], P. Hristov [9], V. Kekelidze, L. Litov, D. Madigozhin, N. Molokanova, Yu. Potrebenikov, S. Stoynev, A. Zinchenko

*Joint Institute for Nuclear Research, Dubna, Russian Federation*

E. Monnier [10], E. Swallow, R. Winston [11],

*The Enrico Fermi Institute, The University of Chicago, Chicago, IL 60126, U.S.A.*

R. Sacco [12], A. Walker

*Department of Physics and Astronomy, University of Edinburgh, JCMB King's Buildings, Mayfield Road, Edinburgh, EH9 3JZ, U.K.*

W. Baldini, P. Dalpiaz, P.L. Frabetti [13], A. Gianoli, M. Martini, F. Petrucci, M. Savrié, M. Scarpa

*Dipartimento di Fisica dell'Università e Sezione dell'INFN di Ferrara, I-44100 Ferrara, Italy*

A. Bizzeti [14], M. Calvetti, G. Collazuol [5], E. Iacopini, M. Lenti, G. Ruggiero [9] M. Veltri [15]

*Dipartimento di Fisica dell'Università e Sezione dell'INFN di Firenze, I-50125 Firenze, Italy*

M. Behler, K. Eppard, M. Eppard [9], A. Hirstius [9], K. Kleinknecht, U. Koch, P. Marouelli, L. Masetti [16], U. Moosbrugger, C. Morales Morales, A. Peters [9], R. Wanke, A. Winhart

*Institut für Physik, Universität Mainz, D-55099 Mainz, Germany* [17]

A. Dabrowski, T. Fonseca Martin [9], M. Velasco

*Department of Physics and Astronomy, Northwestern University, Evanston, IL 60208-3112, U.S.A.*

G. Anzivino, P. Cenci, E. Imbergamo, G. Lamanna [5], P. Lubrano, A. Michetti, A. Nappi, M. Pepe, M.C. Petrucci M. Piccini [9] M. Valdata

*Dipartimento di Fisica dell'Università e Sezione dell'INFN di Perugia, I-06100 Perugia, Italy*

C. Cerri, F. Costantini, R. Fantechi, L. Fiorini [18], S. Giudici, I. Mannelli, G. Pierazzini, M. Sozzi

*Dipartimento di Fisica, Scuola Normale Superiore e Sezione dell'INFN di Pisa, I-56100 Pisa, Italy*

C. Cheshkov, J.B. Cheze, M. De Beer, P. Debu, G. Gouge, G. Marel, E. Mazzucato, B. Peyaud, B. Vallage

*DSM/DAPNIA - CEA Saclay, F-91191 Gif-sur-Yvette, France*

M. Holder, A. Maier [9], M. Ziolkowski

*Fachbereich Physik, Universität Siegen, D-57068 Siegen, Germany* [19]

C. Biino, N. Cartiglia, M. Clemencic, S. Goy Lopez, F. Marchetto, E. Menichetti, N. Pastrone

*Dipartimento di Fisica Sperimentale dell'Università e Sezione dell'INFN di Torino, I-10125 Torino, Italy*

W. Wislicki

*Soltan Institute for Nuclear Studies, Laboratory for High Energy Physics, PL-00-681 Warsaw, Poland*[20]

H. Dibon, M. Jeitler, M. Markytan, G. Neuhofer, L. Widhalm

*Österreichische Akademie der Wissenschaften, Institut für Hochenergiephysik, A-1050 Wien, Austria*[21]

Submitted to Physics Letters B

**Abstract**

The weak radiative decay $\Xi^0 \to \Lambda e^+ e^-$ has been detected for the first time. We find 412 candidates in the signal region, with an estimated background of $15 \pm 5$ events. We determine the branching fraction $\mathcal{B}(\Xi^0 \to \Lambda e^+ e^-) = [7.6 \pm 0.4(\text{stat}) \pm 0.4(\text{syst}) \pm 0.2(\text{norm})] \times 10^{-6}$, consistent with an internal bremsstrahlung process, and the decay asymmetry parameter $\alpha_{\Xi\Lambda ee} = -0.8 \pm 0.2$, consistent with that of $\Xi^0 \to \Lambda\gamma$. The charge conjugate reaction $\overline{\Xi^0} \to \overline{\Lambda} e^+ e^-$ has also been observed.

## 1 Introduction

Since the discovery of hyperons, their (weak) radiative decays have held particular interest [1,2]. Still, the precise nature of the decays themselves remains an open question [3,4].

---

* Corresponding author. *Email address:* prubin@gmu.edu

[1] Present address: Rutherford Appleton Laboratory, Chilton, Didcot, Oxon, OX11 0QX, U.K.

[2] Funded by the U.K. Particle Physics and Astronomy Research Council.

[3] Present address: Massachusetts Institute of Technology, Cambridge, MA 02139-4307, U.S.A.

[4] Present address: Istituto di Cosmogeofisica del CNR di Torino, I-10133 Torino, Italy

[5] Present address: Dipartimento di Fisica, Scuola Normale Superiore e Sezione dell'INFN di Pisa, I-56100 Pisa, Italy

[6] On leave from Österreichische Akademie der Wissenschaften, Institut für Hochenergiephysik, A-1050 Wien, Austria

[7] On leave from University of Richmond, Richmond, VA, 23173, USA; supported in part by the US NSF under award #0140230. Present address: Department of Physics and Astronomy, George Mason University, Fairfax, VA 22030A, USA.

[8] Present address: Dipartimento di Fisica dell'Università e Sezione dell'INFN di Ferrara, I-44100 Ferrara, Italy

[9] Present address: CERN, CH-1211 Genève 23, Switzerland

[10] Present address: Centre de Physique des Particules de Marseille, IN2P3-CNRS, Université de la Méditerranée, Marseille, France.

[11] Also at University of California, Merced, U.S.A.

[12] Present address: Department of Physics, Queen Mary University, London, E1 4NS, U.K.

[13] Present address: Joint Institute for Nuclear Research, Dubna, 141980, Russian Federation

[14] Dipartimento di Fisica dell'Università di Modena e Reggio Emilia, I-41100 Modena, Italy

[15] Istituto di Fisica dell'Università di Urbino, I-61029 Urbino, Italy

[16] Present address: Physikalisches Institut, Universität Bonn, 53113 Bonn, Germany

[17] Funded by the German Federal Minister for Research and Technology (BMBF) under contract 7MZ18P(4)-TP2

[18] Present address: Cavendish Laboratory, University of Cambridge, Cambridge, CB3 0HE, U.K.

[19] Funded by the German Federal Minister for Research and Technology (BMBF) under contract 056SI74

[20] Supported by the Committee for Scientific Research grants 5P03B10120, SPUB-M/CERN/P03/DZ210/2000 and SPB/CERN/P03/DZ146/2002

[21] Funded by the Austrian Ministry for Traffic and Research under the contract GZ 616.360/2-IV GZ 616.363/2-VIII, and by the Fonds für Wissenschaft und Forschung FWF Nr. P08929-PHY

Reliable techniques to predict branching ratios remain elusive. Furthermore, because SU(3) symmetry is broken only weakly in this regime, weak radiative decays should approximately conserve parity [5]. Consequently, the asymmetries of decay angular distributions should be small. However, results from experiments indicate a relatively large (negative) asymmetry in every mode investigated [6]. A number of models have been proposed to explain this apparent discrepancy [7]. Experimental results tend to favor pole models or models based on chiral perturbation theory, which correctly find the sign of the asymmetry. Recently, a resolution of at least part of the puzzle has been offered [8].

When the NA48 Collaboration undertook investigations with a high-intensity $K_S^0$ beam in 2002, trigger strategies for identifying radiative hyperon decays were included from the outset. The production over the full course of the run of more than $3 \times 10^9$ neutral cascades, $\Xi^0(1315)$, offered NA48 unmatched sensitivity for the study of such decays. [1]

This Letter details the measurement with these data of the weak radiative hyperon decay $\Xi^0 \to \Lambda e^+e^-$. This is the first measurement of this decay channel. If one assumes an inner bremsstrahlung-like mechanism producing the $e^+e^-$ pairs, the expected rate for this process may be estimated naively assuming the (virtual) photon converts internally (Dalitz decay) or by using the machinery of QED as carried out in rate predictions for $\Sigma^0 \to \Lambda e^+e^-$ [1,2]. The results give a range from about 1/182 to 1/160 of the rate of $\Xi^0 \to \Lambda\gamma$, or $(6.4 - 7.3) \times 10^{-6}$. Such a process should exhibit a decay asymmetry like that in $\Xi^0 \to \Lambda\gamma$.

## 2 Data

### *2.1 Beam line*

The NA48 beam line was designed to produce and transport both $K_L^0$ and $K_S^0$ beams simultaneously [9]. For the 2002 run, in order to increase dramatically the intensity of the $K_S^0$ beam, the $K_L^0$ target was removed and the $K_L^0$ beamline blocked, the proton flux on the $K_S^0$ target was greatly increased, and a 24 mm platinum absorber was placed after the Be target to reduce the photon flux in the neutral beam. An additional sweeping magnet was installed across the 5.2-meter long collimator, which, tilted at 4.2 mrad relative to the incoming proton beam, selected a beam of long-lived neutral particles ($\gamma$, $n$, $K^0$, $\Lambda$, and $\Xi^0$). In each 4.8 s spill, occurring every 16.2 s, $\sim 5 \times 10^{10}$ protons impinged

[1] The $\overline{\Xi^0}$ production rate was about 1/11 that of $\Xi^0$. This Letter presents numerical results for the $\Xi^0$ only.

on the target. Approximately $2 \times 10^4$ $\Xi^0$s, with momenta between 60 and 220 GeV/$c$, decayed in the fiducial volume downstream of the collimator each spill.

## *2.2 Detector*

The detector for the 2002 run was identical to that used for NA48's measurement of direct CP-violation [9], except that the tagging counter immediately after the last collimator was removed.

### *2.2.1 Decay volume*

The neutral beam exited the final collimation into an evacuated tank, approximately 90 m in length, terminated by a Kevlar window 0.3% of a radiation length thick. The detector was arrayed immediately downstream of this window.

### *2.2.2 Charged particle tracking*

A magnetic spectrometer followed the decay volume. It consisted of four drift chambers, two before and two after an analyzing magnet which provided a transverse momentum kick of 265 MeV/$c$ in the horizontal plane. The chambers were identical, each with two planes of sense wires in four views ($x$, $y$, $u$, $v$). All the chambers were fully instrumented except the third, which had only its $x$- and $y$-views instrumented. Track-time resolution was about 1.4 ns. Space-point resolution was approximately 150 $\mu$m in each projection, and the momentum resolution (with $p$ in GeV/$c$) was:

$$\frac{\sigma_p}{p} = 0.48\% \oplus 0.015\% \times p.$$

The resulting $m_{\pi^+\pi^-}$ resolution in $K_S^0 \to \pi^+\pi^-$ decays was 3 MeV/$c^2$.

### *2.2.3 Electromagnetic calorimetry*

A liquid krypton calorimeter (LKr) detected and measured the energy and position of electromagnetic showers. Its active region was divided transversely into approximately 2 cm $\times$ 2 cm cells, and its depth was 27 radiation lengths. Its single-shower time resolution was less than 300 ps; its transverse position resolution was better than 1.3 mm for a single photon of energy greater than

20 GeV; and its energy resolution [10] was

$$\frac{\sigma(E)}{E} = \frac{3.2\%}{\sqrt{E}} \oplus \frac{9\%}{E} \oplus 0.42\%,$$

where $E$ is in GeV. The resulting $m_{\gamma\gamma}$ resolution in $\pi^0 \to \gamma\gamma$ decays was approximately 1 MeV/$c^2$.

### *2.2.4 Scintillators*

The sensitive region of the electromagnetic calorimeter primarily constrained the fiducial volume of the experiment. Seven rings of scintillation counters bounded, in projection, the edges of this acceptance region, and the last two rings acted as trigger vetoes of extraneous activity.

A scintillator hodoscope, comprised of segmented horizontal and vertical strips arranged in four quadrants and located between the downstream end of the spectrometer and the upstream face of the calorimeter served as a zeroth-level charged-track trigger. Beyond the electromagnetic calorimeter stood an iron-scintillator sandwich hadron calorimeter and three layers of muon counters, each shielded by an iron wall.

### *2.2.5 Trigger and readout*

The entire detector array was sampled every 25 ns. An event trigger initiated a readout of information within a 200 ns window around the trigger time. In this way, time sidebands allowed investigations of accidental activity.

The experiment employed a multi-level trigger designed to maximize flexibility while minimizing pile-up, dead-time losses, and the collection of uninteresting events. To be included in the present analysis, events passed the lowest level hardware trigger if a horizontal-vertical coincidence occurred in at least one quadrant of the scintillator hodoscope, there were no in-time hits in the veto rings, at least three views in the first drift chamber registered more than two hits (as required in the case of more than one track), and either the energy in the electromagnetic calorimeter exceeded 15 GeV or the total energy in the electromagnetic and hadron calorimeters exceeded 30 GeV. The next level trigger required more than one track to have passed through the spectrometer forming one or more good vertices [2]. The highest level trigger, an offline software cull, passed events containing a good $\Lambda$ candidate and at least one

[2] A good vertex is defined, in this context, as the occurrence of two tracks passing within 5 cm of one another between the target and the first drift chamber

high-energy cluster in the calorimeter not associated with either of the tracks forming the $\Lambda$.

A downscaled sample of minimum bias events was collected concurrently with the physics data. Complete trigger information was available for these events, so trigger efficiencies could be measured. The relative fraction of events containing all signal final state particles that passed the required triggers was $\epsilon_{\rm trig}^{\rm sig} = (96.5 \pm 0.2)\%$, while the relative fraction of normalization events ($\Xi^0 \rightarrow \Lambda\pi^0$, $\pi^0 \rightarrow e^+e^-\gamma$) was $\epsilon_{\rm trig}^{\rm norm} = (97.1 \pm 0.2)\%$. This channel was chosen for normalization due to its relative abundance, the similarity of its final state to that of the signal channel, and its selection via the same trigger tree as the signal channel.

### *2.3 Event selection criteria*

Selection criteria were chosen to identify with high efficiency events containing one lambda, one electron, and one positron, all in time. An additional photon was required for the normalization channel.

From events passing all trigger levels, those containing exactly four charged tracks, two of each charge sign, that passed well within the fiducial volumes of the first and fourth drift chambers were kept for further analysis.

Signal event simulation showed that 99% of final state pions, electrons, and positrons had momenta of less than 30 GeV/$c$. A track with momentum greater than 3 GeV/$c$ and associated shower energy within 5% of this momentum was identified as an electron or positron, depending on charge. A (positive) track whose momentum was greater than 30 GeV/$c$ and either had no associated electromagnetic shower or the shower energy to momentum ratio was less than 0.8 was identified as a proton. If no such track was found, or if there were not both an electron and a positron identified, the event was abandoned. If the final track had a momentum greater than 4 GeV/$c$, but not more than 1/3.7 that of the proton track, it was identified as a pion. Otherwise, the event was abandoned.

The tracks associated with the proton and pion had to be separated by at least 5 cm in the first drift chamber and their detection times had to be within 2 ns. If not, the event was abandoned. The distance-of-closest-approach (doca) of the two tracks when projected back towards the target was required to be less than 2.2 cm, and the longitudinal position of this doca had to lie between 4 and 40 meters down stream of the target for the event to be further considered. The momentum vectors of the two tracks were projected, with respect to a reference frame centered on the beam axis, from their positions in the first drift chamber onto the face of the LKr. These projections were weighted by the relativistic energies of the particles associated with the respective tracks, added vectorially, and then normalized to the energy sum of the two particles. The result, a quantity called the center of gravity (COG), had to be greater than 8 cm to ensure that a parent of the two tracks was unlikely to have been directly produced in the target. The COG of a directly produced particle should be small.

The invariant mass of surviving proton and pion candidate pairs was calculated. If the result differed from the nominal mass of the $\Lambda$ by more than 3 MeV/$c^2$ (approximately $3\sigma$), the event was abandoned.

The electron and positron tracks had to have times within 2 ns and a spatial separation in the first drift chamber of at least 2.5 cm. The latter requirement rejects conversions in the Kevlar window. Any unassociated shower in the calorimeter with energy above 1.5 GeV disqualified the event as a signal candidate.

A shower of between 3 and 120 GeV in the electromagnetic calorimeter was considered a photon candidate for the normalization channel if it was unassociated with any track, centered within the fiducial volume of the detector at least 5 cm from a dead cell, and isolated from any other shower.

Finally, for both signal and normalization channels, the event COG, which ideally would be 0 (see above), had to be equal to or less than 6 cm.

A signal (normalization) region was defined as $2\sigma$ either side of the nominal $\Lambda e^+e^-(\gamma)$ invariant mass, where $\sigma_m = 1$ MeV/$c^2$. For the $\Lambda$, the $p\pi$ invariant mass was used. Selection from the entire data set according to these criteria resulted in 412 signal candidates and 29522 normalization events reconstructed.

## 3 Acceptance and reconstruction efficiency

The product of geometrical acceptance ($A$) and selection criteria efficiency ($\epsilon$) was determined with a Monte Carlo simulation. Nearly $10^5$ signal-like events were generated according to a two-body model of a $\Lambda$ and a virtual photon. The model included the decay parameter $\alpha = -0.78$, found for the decay $\Xi^0 \to \Lambda\gamma$ [11], and a $1/m_{ee}^2$ energy distribution for the converting photon, as would be the case for inner conversion. In this way, the model was intended to represent inner bremsstrahlung production. Generated events were stepped through a GEANT simulation of the NA48 detector and analyzed as real data, with the result: $(A \times \epsilon)_{\rm sig} = (2.69 \pm 0.05)\%$. For the normalization channel, about $160 \times 10^6$ events (about $7\times$ the measured flux) were generated with the latest PDG values for the decay parameters incorporated [6]. The result of the detector simulation and reconstruction was $(A \times \epsilon)_{\rm norm} = (0.1251 \pm 0.0003)\%$. Radiative corrections, using PHOTOS [12], were included, as was a $\Xi^0$ polarization of $-10\%$ for signal generation. [3]

## 4 Background

Two sources of background were identified: physics and accidentally in-time combinations.

### 4.1 Physics backgrounds

#### 4.1.1 $\Xi^0 \rightarrow \Lambda\pi^0$

The $\Xi^0$ decays predominantly to $\Lambda\pi^0$. If the $\pi^0$ Dalitz-decays, and the photon goes undetected, the final state is that of the signal. Similarly, if the $\pi^0$ decays via the double-Dalitz mechanism, and an electron and a positron go undetected, the final state is again that of the signal. Finally, the $\pi^0 \rightarrow e^+e^-$ decay results in an irreducible background, but its rate is very small. Simulations of each of these channels at about seven times the flux lead to estimates of $4.6 \pm 0.8$, $0.1 \pm 0.1$, and $1.2 \pm 0.4$ events, respectively, infiltrating the signal region.

#### 4.1.2 Kaon decays

The flux of neutral kaons was an order of magnitude larger than that of the $\Xi^0$. The decay $K^0_S \rightarrow \pi^+\pi^-e^+e^-$ has a branching fraction of $4.7 \times 10^{-5}$. If one of the pions met the requirements of a proton in this analysis, and the resulting $m_{p\pi} \approx m_\Lambda$, then this process would mimic the signal. Simulation with twice the flux of such events demonstrated that an explicit mass cut $| m_{\pi\pi ee} - m_{K^0_S} | > 0.015$ GeV/$c^2$ eliminated essentially any trace of this background with negligible impact on signal-finding efficiency. The decay chain $K^0_L \rightarrow \pi^+\pi^-\pi^0$, $\pi^0 \rightarrow e^+e^-\gamma$, has a product branching ratio of about $1.5 \times 10^{-3}$. The $K^0_L$ lifetime and their typical momentum of 80 GeV/$c$ mean that about 4% of them decay in the experiment's decay volume. For these to become a background to the $\Lambda ee$ signal, a pion would have to be mistaken as a proton and the invariant mass of it combined with that of the other pion would have to be close to that of the $\Lambda$. In addition, the photon would have to go undetected. Because of this last condition, an explicit kaon mass cut would be ineffective in reducing

[3] This polarization value is consistent with that reported by other experiments [13] and with indications from an ongoing study of the NA48 beam.

the background. On the other hand, the efficiency for this chain appearing in the signal region is correspondingly reduced and the COG is smeared out. We estimate on the basis of Monte Carlo simulation that $2 \pm 2$ such events will populate the signal region.

### *4.2 Accidentally in-time combinations*

We estimated the contamination by accidental coincidences four ways:

(1) Running the same analysis on the data, but requiring that the final-state leptons have the same charge.
(2) Requiring that at least one track or shower be between 10 and 20 ns out-of-time and scaling appropriately.
(3) Taking events with $m_{p\pi}$ values between 7 and 10 standard deviations from the central value ($m_{\Lambda}$) and computing $m_{\Lambda ee}$.
(4) Defining two "side-band" regions, one along each axis in COG-versus-$m_{\Lambda ee}$ space [see, in Figure 1, the hatched rectangles at high COG and high mass; each region has the same "area" as the signal region, the open rectangle in the figure].

These approaches, which are not independent, yielded between 1 and 9 events in the signal region; we take the number to be $7 \pm 5$ events.

In conclusion, combining the physics backgrounds with those attributed to accidentals and combinatorics, the estimated number of background events in the signal region is $15 \pm 5$ [see Table 1 for a summary of the background estimation].

Table 1
Sources of expected background events.

| Source | Estimate |
|---|---|
| $\Xi^0 \to \Lambda\pi^0$, $\pi^0 \to e^+e^-\gamma$ | $4.6 \pm 0.8$ |
| $\Xi^0 \to \Lambda\pi^0$, $\pi^0 \to e^+e^-e^+e^-$ | $0.1 \pm 0.1$ |
| $\Xi^0 \to \Lambda\pi^0$, $\pi^0 \to e^+e^-$ | $1.2 \pm 0.4$ |
| Kaon Decays | $2 \pm 2$ |
| Accidentals & Combinatorics | $7 \pm 5$ |
| **TOTAL** | $\mathbf{15 \pm 5}$ |

The background contamination of the normalization sample was estimated from the tails of the $m_{ee\gamma}$ spectrum, which peaks sharply at $m_{\pi^0}$. Including a linear extrapolation under the mass peak, the number was estimated to be $428 \pm 258$.

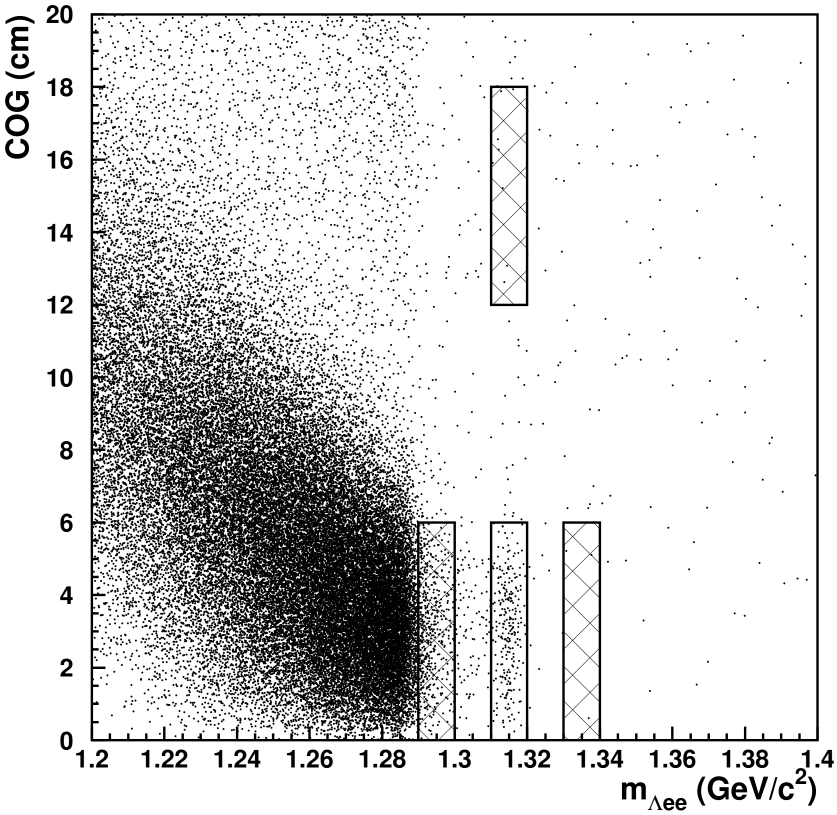


Fig. 1. COG versus $m_{\Lambda ee}$ after all other selection criteria were imposed. The three hatched boxes are side-band regions. The signal region is the open box at low COG around $m_{\Xi^0}$. The side-band regions at high mass-low COG and high COG were used to estimate accidental and combinatoric backgrounds in the signal region. All three side-band regions were used in the subtraction of background under the decay-angle distribution (see text).

## 5 $\Xi^0$ Flux

The total number of $\Xi^0$ produced during the run was estimated by fully reconstructing $\Xi^0 \to \Lambda\pi^0$, $\pi^0 \to e^+e^-\gamma$ events without a longitudinal vertex position cut and using the equation

$$\Phi_{\Xi^0} = \frac{N_{norm} - N_{norm\ bkgd}}{(A \times \epsilon)_{\rm norm}\epsilon_{\rm trig}^{\rm norm}\mathcal{B}(\Xi^0 \to \Lambda\pi^0)\mathcal{B}(\Lambda \to p\pi^-)\mathcal{B}(\pi^0 \to e^+e^-\gamma)} \quad (1)$$

From the entire data set, 29522 such events were reconstructed. After background subtraction, this gives an integrated flux of

$$\Phi_{\Xi^0} = (3.15 \pm 0.03 \pm 0.08) \times 10^9.$$

The first uncertainty is due to statistics, and the second is from branching fraction uncertainties, primarily that on $\mathcal{B}(\pi^0 \to e^+e^-\gamma)$.

Table 2
Quantities that entered into $\Xi^0$ flux calculations.

| | |
|---|---|
| No. of events in signal region | 29552 |
| Estimated no. of background events | $428 \pm 258$ |
| $(A \times \epsilon)_{\rm norm}$ | $(0.1251 \pm 0.0003)\%$ |
| $\epsilon_{\rm trig}^{\rm norm}$ | $(97.1 \pm 0.2)\%$ |
| $\mathcal{B}(\Xi^0 \to \Lambda\pi^0)$ | $0.9952 \pm 0.0003$ |
| $\mathcal{B}(\Lambda \to p\pi^-)$ | $0.639 \pm 0.005$ |
| $\mathcal{B}(\pi^0 \to e^+e^-\gamma)$ | $0.01198 \pm 0.00032$ |

## 6 Results

At the end of the analysis, 412 events were found in the signal region [see Figure 2].

### *6.1 $m_{ee}$ spectrum*

The associated $m_{ee}$ distribution is consistent with a $1/m_{ee}^2$ shape [see Figure 3], and we consider only this model (presumably inner bremsstrahlung) in determining of the branching fraction, including systematic uncertainties.

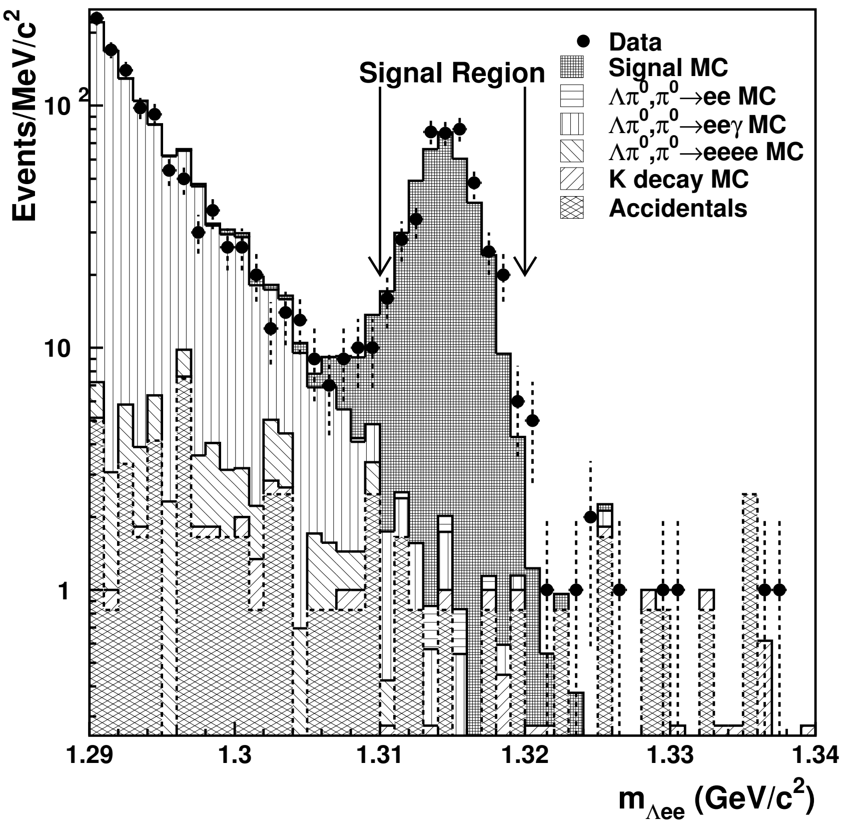


Fig. 2. $m_{\Lambda ee}$ after all selection criteria. Arrows indicate signal region. Stacked in various hatchings (see legend) are the estimated sources of background.

### *6.2 Branching fraction*

Given the background estimate, efficiencies, and flux discussed above, and the PDG $\Lambda \to p\pi^-$ branching ratio [see Table 3], the branching ratio for $\Xi^0 \to \Lambda e^+e^-$ is determined to be

$$\mathcal{B}(\Xi^0 \to \Lambda e^+e^-) = (7.6 \pm 0.4) \times 10^{-6}$$

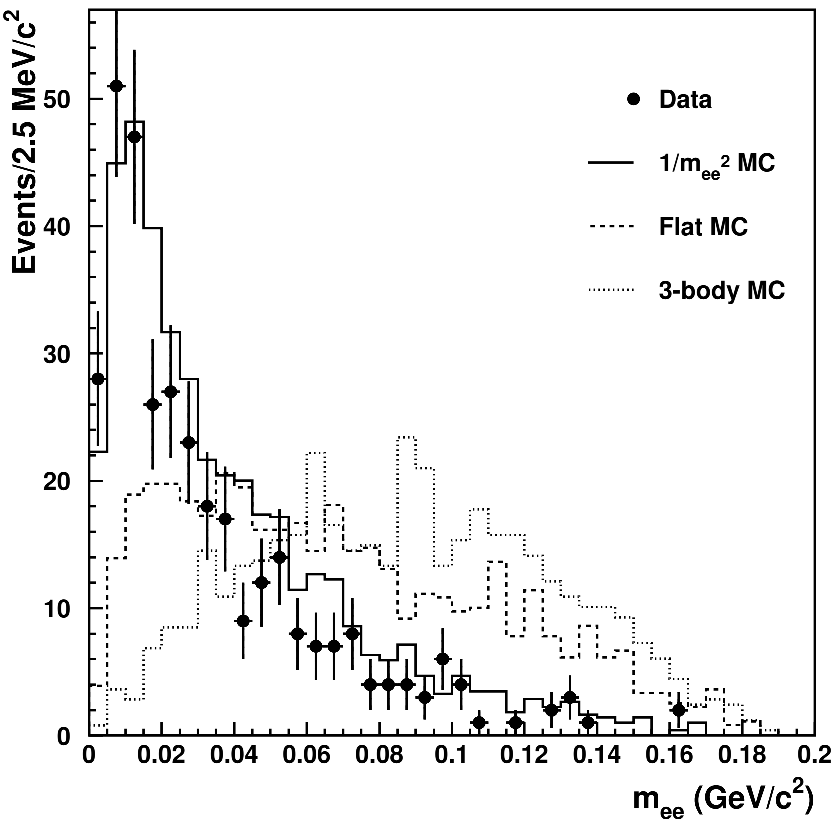


Fig. 3. Reconstructed $m_{ee}$ spectra from data (points), $1/m_{ee}^2$ (solid line), 2-body flat (dashed line), and 3-body phase space (dotted line). The distributions from simulated data have been normalized to the integral of the experimental data. No background subtraction was made on the data.

where the uncertainty here is statistical only.

Anti-cascades also were reconstructed, from $\overline{\Lambda}e^+e^-$ [see Figure 4]. The signal region contains 24 events. Since the anti-cascade has kinematics, backgrounds, and flux that differ from those of the cascade, we undertake no further analysis of this channel here.

Table 3
Quantities that entered into branching fraction calculations.

| | |
|---|---:|
| No. of events in signal region | 412 |
| Estimated no. of background events | $15 \pm 5$ |
| $(A \times \epsilon)_{\text{sig}}$ | $(2.69 \pm 0.05)\%$ |
| $\epsilon_{\text{trig}}^{\text{sig}}$ | $(96.5 \pm 0.2)\%$ |
| $\Xi^0$ flux | $(3.14 \pm 0.03) \times 10^9$ |
| $\mathcal{B}(\Lambda \to p\pi^-)$ | $0.639 \pm 0.005$ |

### *6.3 Systematic uncertainties*

Analysis selection criteria were varied when looking at the data and when determining reconstruction efficiencies. The branching fraction result was most sensitive to the treatment of the reconstructed $\Xi^0$ vertex and backgrounds from the $\Xi^0 \to \Lambda\pi^0$ channel in relation to $m_{ee}$. No cut was placed on the longitudinal position of the $\Xi^0$ vertex. Requirements varying the minimum longitudinal position of the vertex in 6-m intervals beginning before the target (to account for resolution effects) resulted in branching fraction changes of between 0.2% and 3%. We assign the highest variation (±3%) as a systematic error.

It was possible to eliminate nearly all physics backgrounds by excluding signal events with $0.100\ \text{GeV}/c^2 < m_{ee} < 0.135\ \text{GeV}/c^2$, which, according to signal Monte Carlo, reduces the reconstruction efficiency by 5%. Cutting this region from the final data sample, and recalculating the branching ratio, results in a shift of 1.8%, which was included symmetrically as a systematic uncertainty. These, along with smaller variations in the branching fraction resulting from other modifications of the selection criteria, were added in quadrature to give a systematic uncertainty of ±3.6% on the branching fraction.

We conservatively assign a relative ±1% uncertainty on the determination of the background to account for correlations in methods for estimating accidentally in-time events.

The branching fraction differed by about 1% when signal and normalization modes were simulated with and without radiative corrections, and we include this difference symmetrically as a systematic uncertainty.

For the $A \times \epsilon$ determinations, the $\Xi^0$ polarization of simulated events was set to −10%. Samples of simulated data, generated with the polarization varied between 0% and −20% (±10%), were used to recalculate the branching fraction vary. The largest variation among these trials was 2.7%, and this variation is taken symmetrically as a systematic uncertainty.

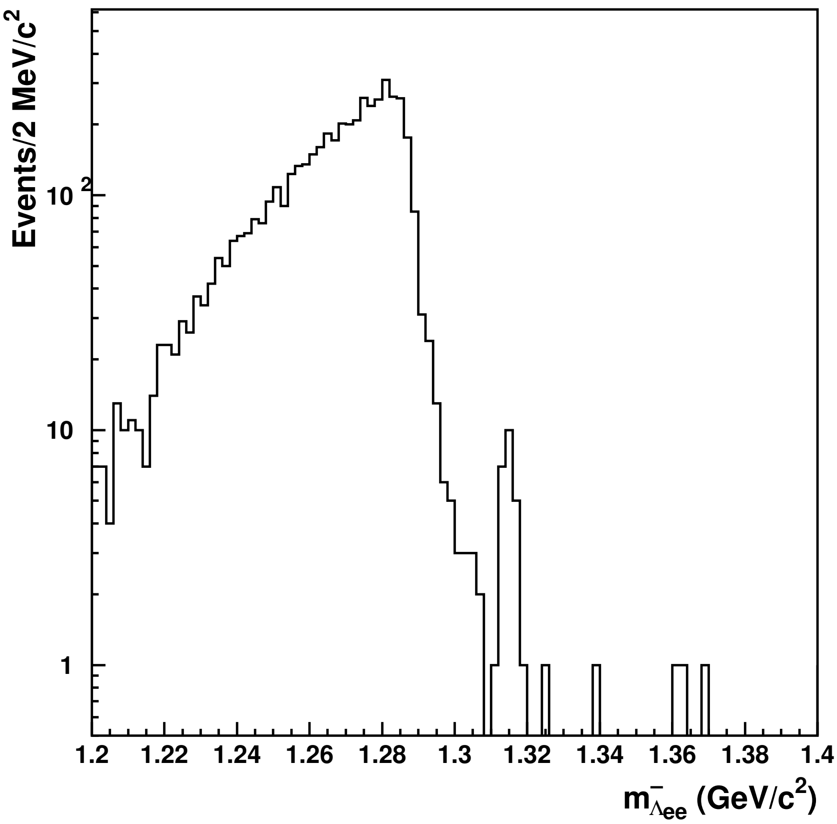


Fig. 4. The $m_{\overline{\Lambda}ee}$ spectrum after all cuts.

The decay asymmetry used in generating simulated signal events was that of the process $\Xi^0 \to \Lambda\gamma$ [11]. Our measurement, discussed below, is in agreement with this value, but with a 25% uncertainty. Varying our simulation within this 25% range changed the branching fraction by at most 2.5%, and this is symmetrically assigned to systematic uncertainty.

The determination of the trigger efficiency and $\Xi^0$ flux were discussed above. The difference between trigger efficiencies for signal and normalization channels is taken as an uncertainty, affecting the branching ratio by 0.6%. An alternative, less direct, calculation of the flux was statistically consistent with the one described above. The two differed by 1.9%, and we conservatively include, symmetrically, this amount as a systematic uncertainty.

The total systematic uncertainty on the branching fraction, recounted in Table 4, is ±5.7%, the sum in quadrature of each of the sources described. This gives a final branching fraction of:

$$\mathcal{B}(\Xi^0 \rightarrow \Lambda e^+ e^-) = [7.6 \pm 0.4(\text{stat}) \pm 0.4(\text{syst}) \pm 0.2(\text{norm})] \times 10^{-6}.$$

Table 4
Sources of systematic uncertainty on the branching fraction.

| Source | Fractional Uncertainty |
|---|---|
| Detector Acceptance | 3.6% |
| Background | 1.0% |
| Radiative Corrections | 1.0% |
| Polarization | 2.7% |
| Signal Modeling | 2.5% |
| Trigger Efficiency | 0.6% |
| $\Xi^0$ Flux | 1.9% |
| **TOTAL** | **5.7%** |

### *6.4 Asymmetry parameter*

The angular distribution of the proton relative to the $\Xi^0$ line of flight in the $\Lambda$ rest frame is given by [6]:

$$\frac{dN}{d\cos\theta_{p\Xi}} = \frac{N}{2}(1 - \alpha_{\Xi\Lambda ee}\alpha_{\_}\cos\theta_{p\Xi}). \qquad (2)$$

The $\cos\theta_{p\Xi}$ spectrum from signal events was corrected by subtracing scaled backgrounds from the side-band regions indicated in Figure 1 and by dividing, bin-by-bin, the acceptance as determined from a $\Xi^0 \rightarrow \Lambda e^+ e^-$ simulation where the spectrum was generated to be flat in $\cos\theta_{p\Xi}$. A two-parameter fit to this corrected spectrum gives the product of asymmetry parameters $\alpha_{\Xi\Lambda ee}\alpha_{\_}$, where $\alpha_{\_}$ is the asymmetry parameter for the decay $\Lambda \rightarrow p\pi^-$. This latter was taken to be $\alpha_{\_} = 0.642 \pm 0.013$ [6]. The fit (over the interval $-0.8 < \cos\theta_{p\Xi} < 1$)

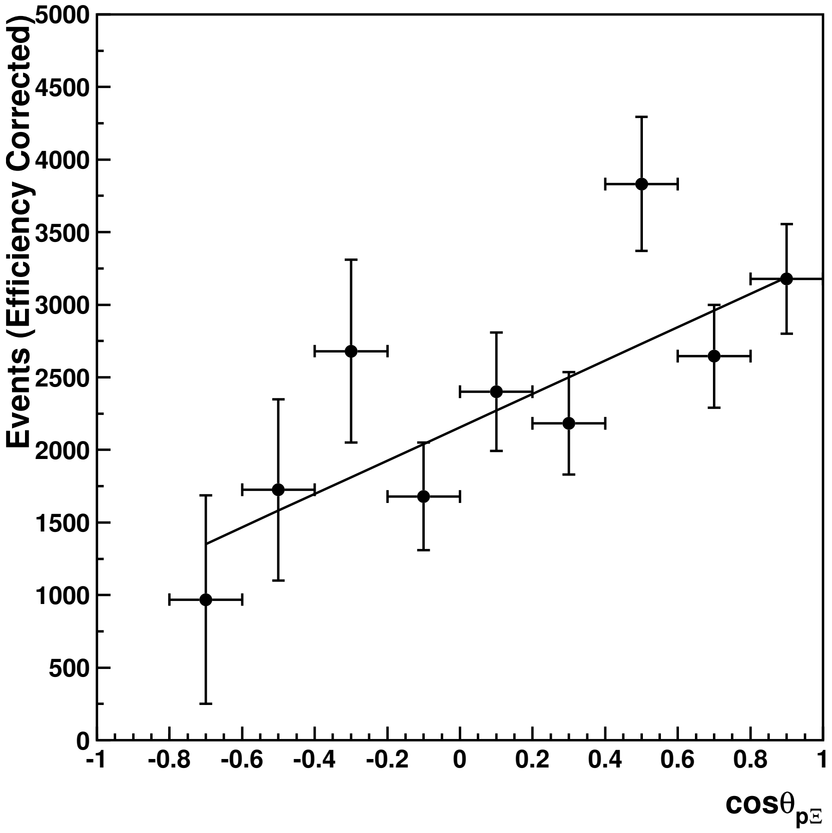


Fig. 5. Background-subtracted and acceptance-corrected $\cos\theta_{p\Xi}$ distribution. The line is the fit result.

[see Figure 5] to the data yields,

$$\alpha_{\Xi\Lambda ee} = -0.8 \pm 0.2$$

This is consistent with the latest published value of $\alpha_{\Xi\Lambda\gamma} = -0.78{\pm}0.18(\text{stat}){\pm}0.06(\text{syst})$ [11].

## 7 Summary and conclusions

The weak radiative decay channel $\Xi^0 \to \Lambda e^+e^-$ has been identified. Its branching fraction has been determined to be

$$\mathcal{B}(\Xi^0 \to \Lambda e^+e^-) = [7.6 \pm 0.4(\text{stat}) \pm 0.4(\text{syst}) \pm 0.2(\text{norm})] \times 10^{-6},$$

consistent with an inner bremsstrahlung-like production mechanism for the $e^+e^-$ pair. The consistency is further supported by the $m_{ee}$ spectrum. The decay parameter

$$\alpha_{\Xi\Lambda ee} = -0.8 \pm 0.2,$$

is consistent with that measured for $\Xi^0 \to \Lambda\gamma$.

Twenty four events of the charge conjugate reaction $\overline{\Xi^0} \to \overline{\Lambda}e^+e^-$ populate the nominal signal region. This number is consistent with the $\Xi^0$ branching fraction and the relative $\Xi^0$ and $\overline{\Xi^0}$ production rates.


## Acknowledgments

It is a pleasure to thank technical personnel from participating laboratories and universities, and affiliated computer centers, for their essential contributions to constructing the apparatus, running the experiment, and processing the data.


## References


[1] J. Bernstein, G. Feinberg, and T. D. Lee, Phys. Rev. **139**, 1650 (1965).

[2] G. Feldman and T. Fulton, Nucl. Phys. B **8**, 106 (1958).

[3] J. Lach, P. Żenczykowski, Int. J. Mod. Phys. A**10**, 3817 (1995).

[4] D. A. Jensen, Nucl. Phys. B (Proc. Suppl.) **93**, 22 (2001).

[5] Y. Hara, Phys. Rev. Lett. **12**, 378 (1964).

[6] W.-M. Yao et al. (Particle Data Group), J. Phys. G **33**, 1 (2006) (URL: http://pdg.lbl.gov)

[7] P. Żenczykowski, Phys. Rev. D **62**, 014030 (2000), and references therein.

[8] P. Żenczykowski, hep-ph/0610191.

[9] J. R. Batley, et al., Phys. Lett. B **544**, 97 (2002).

[10] NA48 Collaboration, G. Unal, in: IX International Conference on Calorimetry, October 2000, Annecy, France, hep-ex/0012011.

[11] A. Lai, et al., Phys. Lett. B **584**, 251 (2004).

[12] E. Barberio and Z. Was, Comput. Phys. Commun. **79**, 291 (1994).

[13] E. Abouzaid, et al., hep-ex/0608007.